Fermi National Accelerator Laboratory

FERMILAB-Conf-96/273

Design Formulas for the Strength, Compensation and Trimming of Hybrid Permanent Magnets

Bruce C. Brown

Fermi National Accelerator Laboratory
P.O. Box 500, Batavia, Illinois 60510

October 1996

Presented at the *DPB Mini Symposium: Permanent Magnets, Meeting of the American Physical Society*, Indianapolis, Indiana, May 2-5, 1996.

Operated by Universities Research Association Inc. under Contract No. DE-AC02-76CH03000 with the United States Department of Energy

Disclaimer

This report was prepared as an account of work sponsored by an agency of the United States Government. Neither the United States Government nor any agency thereof, nor any of their employees, makes any warranty, express or implied, or assumes any legal liability or responsibility for the accuracy, completeness or usefulness of any information, apparatus, product or process disclosed, or represents that its use would not infringe privately owned rights. Reference herein to any specific commercial product, process or service by trade name, trademark, manufacturer or otherwise, does not necessarily constitute or imply its endorsement, recommendation or favoring by the United States Government or any agency thereof. The views and opinions of authors expressed herein do not necessarily state or reflect those of the United States Government or any agency thereof.

Distribution

Approved for public release: further dissemination unlimited.

Doc Number:
FERMILAB/Conf-96/273
Version: 1.1

Design Formulas for the Strength, Compensation and Trimming of Hybrid Permanent Magnets

Bruce C. Brown
Accelerator Division/Main Injector Department
*Fermi National Accelerator Laboratory**
P.O. Box 500
Batavia, Illinois 60510

10/25/96

*Operated by the Universities Research Association under contract with the U. S. Department of Energy

Contents

Abstract

Hybrid permanent magnets provide an economical source of fixed-strength magnets. The field shape is controlled by the shape and position of iron poletips while the strength is determined by geometry and the quantity and quality of the permanent magnetic materials. We will derive here simple formulas for calculating the strength of simple hybrid magnets when driven by materials with linear B-H curves in the region of interest (CSEM). We will also show how to tune the strength by shunting flux with iron shims to change gap heights. The same calculational techniques will allow design of temperature compensation based on shunting flux in a temperature dependent fashion using ferromagnetic materials with a low Curie temperature[1].

1 Magnet Strengths - An Introduction

For most simple accelerator electromagnets, one separates the design problem into a body field calculation which can be carried out very accurately with a two dimensional code and a small end contribution. The body field strength can be easily determined analytically to at least 0.1% from examination of the design geometry (for intermediate currents where neither remanent field nor iron saturation are important). The situation for permanent magnets is different. If only the simplest portions of the geometry are considered, the field strength will not be known with even a few percent accuracy. But a careful analysis of the problem for important simple geometries allow a complete design of the strength, including end effects, to a useful precision. In its simplest form, such an analysis will assume that all iron in the problem creates magnetic equipotentials. Using CSEM [2] to excite the poles, one can determine the magnetic potential and the resulting magnetic fields from the strength of the CSEM materials and the geometric properties of the magnet. We will consider cases in which the dominant effects are

[1]This work expands upon a presentation at the DPB Mini Symposium:Permanent Magnets, Meeting of the Am. Phys. Society at Indianapolis, Indiana, May 2-5, 1996[1]

[2]With CSEM we denote either Current Sheet Equivalent Materials or Charge Sheet Equivalent Materials. These are permanent magnetic materials whose differential permeability is small (nearly 1) and quite constant at various excitation levels. One can represent these materials quite accurately with either a current sheet or a charge sheet on the appropriate boundary. Materials which are described well as CSEM include hard ferrites such as those of Sr and Ba, samarium-cobalt ($SmCo_5$) and neodymium-iron-boron ($Nd_2Fe_{14}B$). Information on commercial grades of these materials and their properties is available from the Magnetic Materials Producers Association[2].

due to the rectangular regions for the permanent magnet materials and either rectangular (dipole) or simple multipole (quadrupole, sextupole...) pole tips. Gradient magnets can be calculated as minor perturbations from the geometry of dipoles.

Simple extensions of these ideas provide the formulas which will allow us to provide strength tuning shunts and temperature compensation shunts. Related results will provide guidance on the effects of geometrical defects such as gaps or CSEM materials which drive direct fields. An exact calculation[3] of a rectangular dipole is considered in the next section. The calculational techniques are introduced in the Appendix.

This work is motivated by the current Fermilab effort in permanent magnets[3]. This includes an 8 GeV transfer line from the Fermilab Booster to the Main Injector. Dipoles for this line are currently under construction. A design has been proposed for the Recycler Ring[4], a storage and cooling ring for anti-protons to be built in the same tunnel as the Main Injector.

2 Strength Calculation for a Rectangular Dipole

Dipole magnets which are constructed in the form shown in Figure 1 provide a bending field which is vertical in the gap shown at the bottom of the figure. We derive relationships which are assumed to apply along a length L_{mag} of the pole. Assuming that the poletip is an equipotential surface, we find the field in a gap of half height g_h is given by $B_y = \mu_0 V_m / g_h$. We calculate the magnetic scalar potential V_m using Ampere's Law and the conservation of flux (ϕ). We first apply flux conservation to the surface of the poletip. We describe the magnetic fields in each flux bundle as positive when directed into the iron surfaces of the pole. We divide the surface into a number of separate areas, A_i, and observe that

$$\sum \phi_i = 0. \tag{1}$$

On the rectangular (in three dimensions) surfaces, we assume that there is a uniform transverse field, B_i so that $\phi_i = A_i B_i$ with $A_i = w_i L_{mag}$. Additional flux which goes to regions beyond the corners is associated with each edge, j, of these rectangular surfaces. It is added separately and labeled

[3]We will use SI units for all calculations. For convenience of those used to CGS (Gaussian) units, we will frequently quote numerical results and measurements in both units. In addition, we will avoid the confusion of the SI units for H by quoting both B and $\mu_0 H$ in Tesla. These are converted to CGS units by multiplying by 10^4.

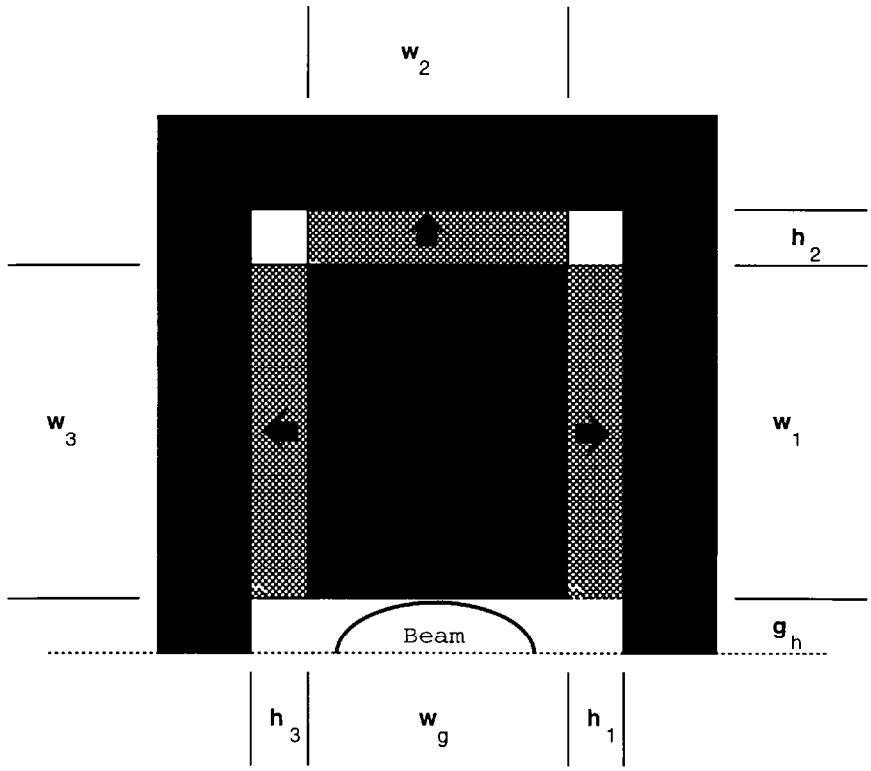

Figure 1: Schematic end view (upper half) of a permanent magnet hybrid dipole. Iron is shown in black. CSEM is cross-hatched grey. Arrows indicate the direction of magnetization of the material. The useful volume is in the gap above the centerline (shown at the bottom of the illustration). A beam pipe is shown to draw attention to this working gap where a vertical field is produced. The pole tip is the iron block above the gap. Top, bottom, and side plates are iron for flux return. Field is driven by bricks of CSEM (ferrite) material placed between the flux return plates and the pole tip. In the beam direction (direction of view), the magnet has length L_{mag}. (To facilitate a general notation in the equations we show two dimensions with different labels. $w_3 = w_1, w_g = w_2$.)

"excess" flux, ϕ_{ej}. The excess flux is proportional to the pole potential and the length, L_j of the edge to which it applies, $\phi_{ej} = E_j L_j \mu_0 V_m$, where E_j is called the excess flux coefficient. If permanent magnet materials are used to drive flux at the ends of the magnet, they are added in the same fashion while the flux directed from the end covers can be separated into "ideal" and "excess" flux in the same fashion as in other portions of the magnet. Thus

$$\sum \phi_i = \sum A_i B_i + \sum \phi_{ej} = \sum A_i B_i + \sum E_j L_j \mu_0 V_m = 0. \qquad (2)$$

We use Ampere's Law to relate the H in each gap to the pole potential.

$$\frac{B_g g_h}{\mu_0} - h_i H_i = 0, \qquad (3)$$

where we have assumed the $H = 0$ in the iron.

The additional constraints required to solve the above equations are provided by the B-H relations (constitutive equations) for the materials in each region of the magnet assembly. In the air (or vacuum) gaps, we have $B = \mu_0 H$. For CSEM we assume $B = B_r + \mu_r \mu_0 H$. Data for a strontium ferrite sample is shown in Figure 2. If we solve for H_i in Equation 3 and substitute the result into the constitutive equation for the material in each gap we have a formula for the B_i.

$$B_i = B_{ri} + \mu_{ri} \mu_0 H_i = B_{ri} + \mu_{ri} \mu_0 \frac{B_g g_h}{\mu_0 h_i} \qquad (4)$$

which can be substituted back into the flux conservation formula.

$$\sum A_i (B_{ri} + \frac{\mu_{ri}}{h_i} B_g g_h) + \sum E_j L_j \mu_0 V_m = 0. \qquad (5)$$

We will separate the equation into source terms and flux transport terms:

$$\sum A_i B_{ri} + \sum \frac{A_i \mu_{ri}}{h_i} B_g g_h + \sum E_j L_j \mu_0 V_m = 0 \qquad (6)$$

$$\mu_0 V_m = B_g g_h = -\frac{\sum A_i B_{ri}}{\sum \frac{A_i \mu_{ri}}{h_i} + \sum E_j L_j} \qquad (7)$$

In a following section we examine excess flux coefficients which apply to this geometry. In general, one can evaluate the "excess flux" terms by

- analytic calculations

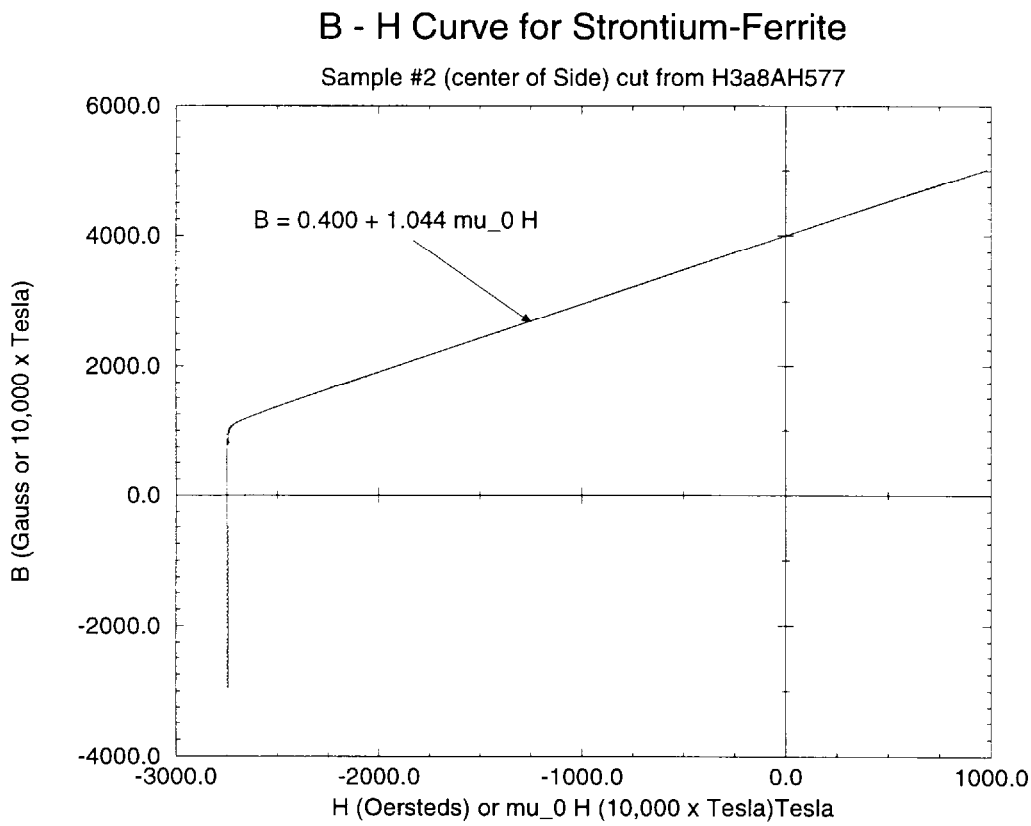

Figure 2: Measured B-H curve for sample of oriented strontium ferrite (Ceramic 8) CSEM. Measurement by KJS Associates, Inc. Fitted results include $B_r = 0.4T(4.00kG)$, $\mu_0 H_{ci} = 0.27T(H_{ci} = 2.74Oe)$, $\mu_0 BH_{max} = 3.83 \times 10^{-2}T^2(BH_{max} = 3.83MGOe)$.

- 2-D Calculation using magnet analysis code (POISSON or PE2D or...).

The terms of form $\mu_{ri}A_i/h_i$ are called the permeance (P) of the gap i (*cf.* McCaig[5], page 197) whereas $h_i/\mu_{ri}A_i$ is called reluctance[4](R). Note that the effect of μ_r is to modify the effect of the space between equipotentials, creating an effective height $h' = h/\mu_r$. Since we have several permeances in parallel, we add them as shown. This geometrical property determines the distribution of flux.

We find useful analogs for these calculations in the more familiar calculations for electrical quantities. In the analog resistive circuit, we represent the permeance with a conductance. The analog of the voltage is the magnetic potential (or magneto-motive force) and the current is the analog of the flux. In the electrical analog, this dipole is equivalent to a parallel resistive network driven by a current source where the voltage achieved depends upon the net conductance of the attached network. Hybrid magnets with no electric coils have a fixed flux available given by $\sum A_i B_{ri}$. The magnetic potential (or magneto-motive force) is determined by the flux available and the permeance of the circuit.

An even more useful electrical analog is provided by observing the analogy between Equation 7 and the familiar formula for the voltage of a set of capacitors in parallel,

$$V = \sum \frac{Q_i}{C_i}. \tag{8}$$

Capacitance (C) a good analog for permeance (P) in this application. In more complex applications with additional magnetic equipotentials, the analogy is especially valuable.

3 Formulation to Solve General Permanent Magnet Fields

To formulate a general solution to the problem of the magnetic fields produced by an array of iron surfaces and a collection of CSEM materials, we consider CSEM as charge sheet equivalent material. Following Halbach (Insertion Device Design[6], page 4.13) we consider an approach which guides

[4] Most authors define reluctance with respect to the average μ (in the sense of $B = \mu H$) whereas, for calculations using CSEM and iron which is not in saturation, we see that using linear approximations to the B-H curve and using the differential or recoil μ is more useful.

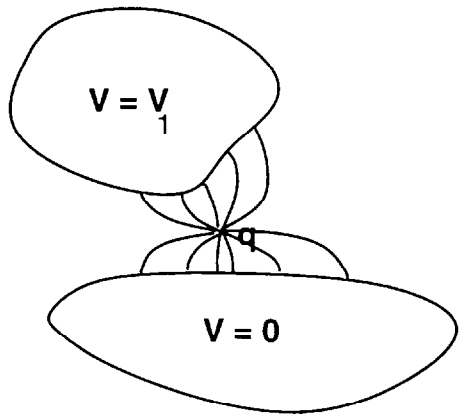

Figure 3: General Geometry for Hybrid Magnet with two surfaces and one magnetic charge. Even when we represent the effects of a CSEM material by magnetic charges, we will not find isolated charges when the full problem is considered.

the general solution for problems of permanent magnet design. We assume the general constitutive equation for the CSEM to be

$$\vec{B} = \vec{B_r} + \mu_0 \hat{\mu} \times \vec{H}. \tag{9}$$

where $\hat{\mu}$ is a tensor which is diagonal when one axis is chosen parallel to the easy axis of magnetization. We denote the magnetic easy axis by $_{||}$.

$$\nabla \cdot \vec{B} = 0 = \nabla \cdot \vec{B_r} + \nabla \cdot \mu_0 \hat{\mu} \times \vec{H} \tag{10}$$

$$\nabla \cdot \mu_0 \hat{\mu} \times \vec{H} = -\nabla \cdot \vec{B_r} = \rho_m \tag{11}$$

We observe that the CSEM determines the value of $\vec{H}$ through $\mu_{||}, \mu_{\perp}$ and the charge density ρ_m. When B_r is uniform in the volume of the CSEM, then ρ_m will be non-zero only at the surfaces.

We will construct two solutions whose difference is the desired general solution outside the iron. By linear superposition, we may consider a point charge and 2 iron surfaces as shown in Figure 3 and generalize from that solution.

- Solution 1 has fields created directly by the charges ($\rho_m \neq 0$) but has potential $V_m = 0$ on all surfaces. The solution is represented by a

scalar potential $V_q(\vec{r})$ and a magnetic field $\vec{H}_q(\vec{r}) = \vec{\nabla} V_q$. The resulting flux emanating from surface 1 is $\phi_q = \int_1 \mu_o \vec{H}_q \cdot d\vec{a} = c_1 q$, where c_1 is a constant to be determined. We call these the direct fields from charge q.

- Solution 2 has potential V_{s0} on surface 1 but $\nabla \cdot \vec{B}_r = 0$ (no magnetic charge) everywhere outside the iron. The solution is represented by a scalar potential $V_s(\vec{r})$ and a magnetic field $\vec{H}_s(\vec{r}) = \vec{\nabla} V_s$. The resulting flux emanating from surface 1 is $\phi_s = \int_1 \mu_o \vec{H}_s \cdot d\vec{a} = c_2 V_{s0}$, where c_2 is another constant to be determined. We call these the indirect fields.

- We construct the desired solution from these by demanding that the flux created by the charges in solution 1 be canceled on the surface of body 1 by the flux created by solution 2. For this single charge, the solution is $V = V_q - V_s$. $\vec{H}(\vec{r}) = \vec{H}_q(\vec{r}) - \vec{H}_s(\vec{r})$. The net flux from surface 1 is $\phi = 0 = \phi_q - \phi_s = q c_1 - V_{s0} c_2$.

3.1 Solution to Direct Fields: Point Magnetic Charge

We will demonstrate here that the constant $c_1 = V_s(\vec{r})/V_{s0}$. Consider

$$I = \int_{All\ S} (V_s \vec{B}_q - V_q \vec{B}_s) d\vec{a} \tag{12}$$

where the integral is over the surface of all iron in the problem. On surface 0 (the potential reference) $V_q = V_s = 0$. On surface 1, $V_q = 0$, $V_s = V_{s0}$. On the surface at ∞, $V\vec{B}$ goes to zero faster than the area goes to ∞, thus giving no contribution to the integral. We are thus left with (for the problem with two iron surfaces)

$$I = \int_{S1} V_s \vec{B}_q d\vec{a} = V_{s0} \phi_q. \tag{13}$$

Consider now

$$\nabla \cdot (V_s \vec{B}_q - V_q \vec{B}_s) = V_s \nabla \cdot \vec{B}_q - V_q \nabla \cdot \vec{B}_s + \vec{H}_q \cdot \vec{B}_s - \vec{H}_s \cdot \vec{B}_q. \tag{14}$$

We note that

$$\nabla \cdot \vec{B}_q = \rho_m \quad , \nabla \cdot \vec{B}_s = 0, \tag{15}$$

the first by definition, the second by our assumption about the second solution.

$$\frac{1}{\mu_0} \vec{H}_q \cdot \vec{B}_s = (\vec{H}_{q||} + \vec{H}_{q\perp}) \cdot (\mu_{||} \vec{H}_{s||} + \mu_\perp \vec{H}_{s\perp}) = \vec{H}_{q||} \cdot \mu_{||} \vec{H}_{s||} + \vec{H}_{q\perp} \cdot \mu_\perp \vec{H}_{s\perp}. \tag{16}$$

By symmetry, we see that

$$\vec{H}_q \cdot \vec{B}_s = \vec{H}_s \cdot \vec{B}_q, \tag{17}$$

allowing us to cancel the final terms in Equation 14. Returning to Equation 12, we convert the surface integral of the argument to a volume integral over the divergence of that argument,

$$I = \int_{All\ S} (V_s \vec{B}_q - V_q \vec{B}_s) d\vec{a} = \int_{Vol} V_s(\vec{r}) \rho_m(\vec{r}) \tag{18}$$

Taking advantage here of the fact that we are considering only a point charge, we find

$$I = V_s(\vec{r}) q \tag{19}$$

Since

$$I = V_s(\vec{r}) q = V_s \phi_q. \tag{20}$$

We thus have

$$\phi_q = \frac{V_s(\vec{r})}{V_{s0}} q, \tag{21}$$

proving the hypothesis of this subsection.

3.2 Constructing Useful Solutions

Since no real magnetic charges exist, the solution above is only useful when combined by linear superposition to provide the solution when there is a set of charges. For each set of charges, the resulting potentials, V_{s0}, define the indirect fields. These need to be calculated by solving for $V_s(\vec{r})$ and calculating $c_2 = \frac{\phi_s}{V_{s0}}$.

When considering the entire surface of body 1, we know that for any solution of magnetostatic Maxwell's Equations, the next flux will be zero. Although we have demonstrated a mathematical separation into direct and indirect fields, the resulting understanding comes with a pair of added observations.

- We often will place CSEM so that the surface touches the iron. In fact in the examples above, all CSEM was so placed. By examining regions which include part of the CSEM and the adjacent iron, we find an apparent charge "on the surface" of the iron.
- Useful calculating tools will not always consider the entire volume of a problem but instead will use inner boundaries and appropriate boundary conditions.

By dividing problems into regions with the considerations mentioned above, we are ready to find general solutions. One further consideration makes most problems not only possible but quite tractable: In regions far from the sources, the direct fields decay exponentially with a characteristic length governed by the spacing between iron surfaces.

4 Formulas for Excess Flux Coefficients

Calculation of indirect field contributions is simplified considerably by the concept of excess flux coefficients introduced above. In the portion of the geometry where the equipotential surfaces are parallel, the dominant field con-

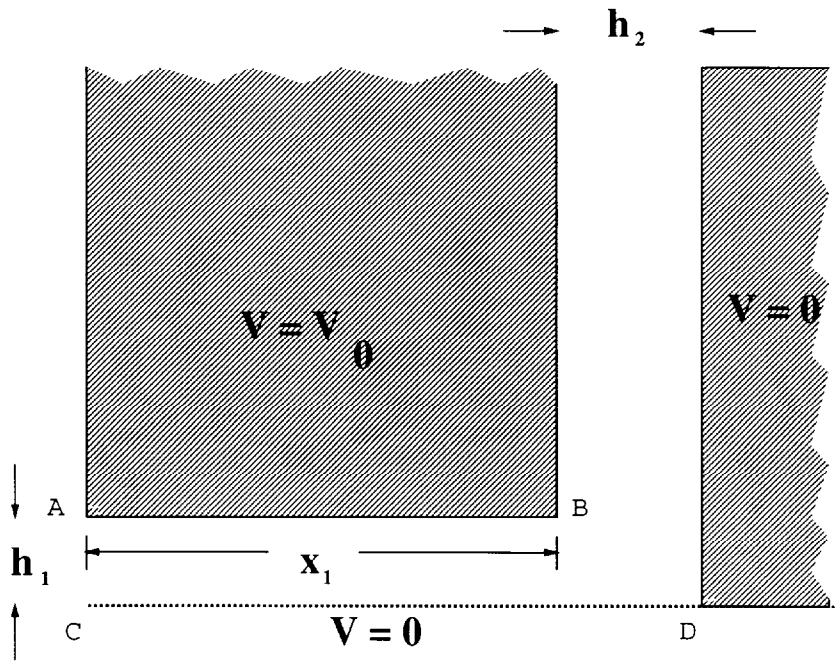

Figure 4: Illustration of geometry at corner of a magnet pole for calculation of "excess" flux. The iron at potential V_0 is a pole for the magnet. The line CD is a symmetry plane of the magnet and is at potential $V = 0$. We assume that this is a cross section for a portion of magnet of length L in the direction of view where L is large compared to h_1 or h_2, such that a two dimensional calculation is appropriate.

tribution is a uniform transverse field. A non-uniform contribution, which is largest at the corner, dies exponentially with the distance into the gap. Beyond the corner, the field is governed by the same potentials but is quite non-uniform. We present here the formulas for the flux contribution of these fields.

Consider a two dimensional view of a dipole magnet as shown in Figure 4. We see the right upper portion of the cross section with the dashed horizontal line marking the vertical (top-bottom) symmetry plane. The upper half of the gap is of height h_1 with the half pole extending from A to B and having width x_1. The return yoke is shown along the right side and is separated from the poletip by a gap h_2. The calculation[5] sums contributions of flux from the uniform field (vertical) which exits from the pole between A and B, and a term which accounts for the flux which exits the pole from that side but passes to the right, either at a wider point on the mid-plane C-D or into the return yoke iron to the right.

We assume that the magnetic potential of the pole is $V = V_0$ where we have assigned the potential 0 to the return yoke. The potential along the horizontal mid-plane (line from C to D) will also be $V = 0$.

We require the flux ϕ_{AB} (excess flux at the pole)[6] which passes through the lower boundary of the pole between points A and B. It is given by

$$\phi_{AB} = \mu_0 V_0 (\frac{x_1}{h_1} + E_{AB}) \tag{22}$$

with

$$E_{AB} = \frac{1}{\pi}(\ln \frac{1 + \frac{1}{a^2}}{4} + 2a \arctan \frac{1}{a}), \tag{23}$$

where $a = h_1/h_2$.

The flux which passes through the gap between C and D (excess flux at the symmetry plane) is governed by similar equations

$$\phi_{CD} = \mu_0 V_0 (\frac{x_1}{h_1} + E_{CD}) \tag{24}$$

where

$$E_{CD} = E_{AB} + \frac{2}{\pi} \ln a. \tag{25}$$

[5]The results reported in this section are given without derivation. They were provided from class notes distributed by Dr. Klaus Halbach at the US Particle Accelerator School classes on magnet design. I thank Dr. Ross Schlueter for help in obtaining this material and Dr. Halbach for reviewing my presentation of it.

[6]Be sure to note that the flux calculated in this section is for the two dimensional case. To obtain a 'real' flux in $T\text{-}m^2$ one must multiply by the magnet length, L_{mag}.

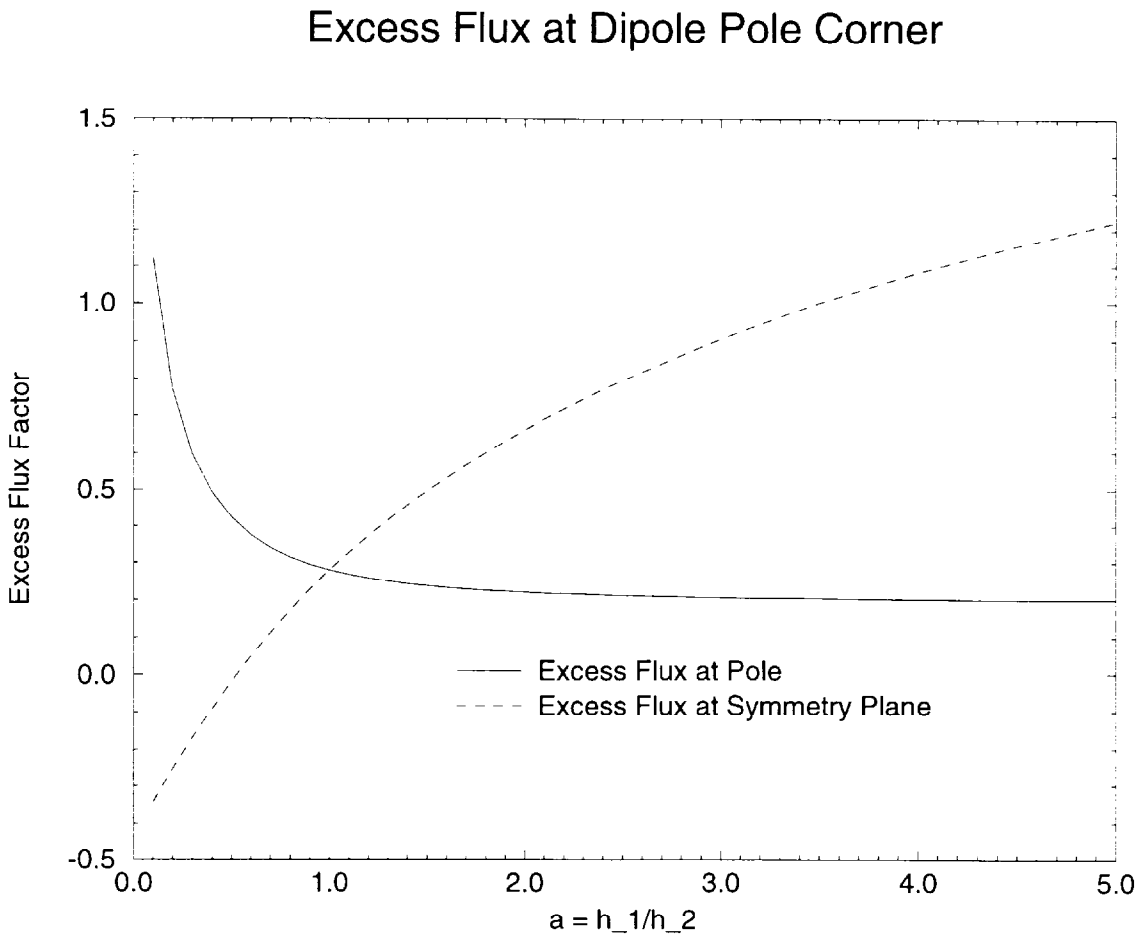

Figure 5: Excess Flux Factor is shown as a function of the ratio of gap over side spacing.

We identify the term x_1/h_1 as the 'ideal' flux coefficient and E_{AB} (E_{CD}) as the 'excess' flux coefficient.

Note that the flux passing through the right side of the pole above point B is governed by an 'ideal' flux coefficient plus an 'excess' flux coefficient given by E_{AB} with the substitution $a' = 1/a$. In Figure 5 we have plotted the values of E_{AB} and E_{CD} as a function of a.

The case where $h_1 = h_2$ ($a = 1$) provides an instructive example.

$$E_{AB} = \frac{1}{\pi}(\ln \frac{1}{2} + 2 \arctan 1) = .2793 \qquad (26)$$

$$\phi_{AB} = \mu_0 V_0 (\frac{x_1}{h_1} + .2793) \tag{27}$$

Note that this excess flux is equivalent to the contribution of a portion of the pole of width $.2793 h_1$. Note that $E_{AB} = E_{CD}$.

5 Temperature Compensation

The properties of ferromagnetic materials are temperature dependent:

- The saturation magnetization, M, at temperature T is described by a Curie Law.
$$\frac{M}{M_0} = \tanh \frac{M/M_0}{T/\theta_c}, \tag{28}$$
where θ_c is the Curie Temperature and M_0 is the saturation magnetization at zero temperature.

- The magnetization at fixed high H (above the "knee" of the M-H curve, where the slope drops to near 0) is still well described by the the Curie Law.

- Upon examination, one will find that as a consequence, at a fixed temperature the value of
$$\frac{1}{M}\frac{dM}{dT} \tag{29}$$
is almost uniquely determined by the Curie temperature.

- The Curie temperature of strontium ferrite is about 450^o C. This gives a room temperature value of
$$\frac{1}{M}\frac{dM}{dT} \sim -0.002/^oC. \tag{30}$$

We wish to use temperature compensation alloy to cancel the strength reduction caused by the lower flux produced by the ferrite when the temperature rises. We choose an alloy for which the temperature coefficient is much larger than the one for ferrite (one with lower Curie Temperature). We place it in the magnet structure so that it subtracts from the flux on the pole. When the temperature rises, the compensator will steal less flux as the ferrite produces less flux.

As an example geometry, Figure 6 is a side view of the upper portion of a magnet. We install temperature compensation materials periodically

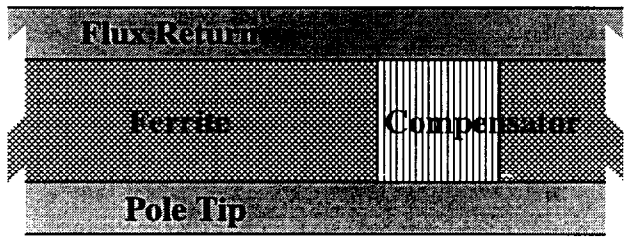

Figure 6: Magnet Assembly side view with temperature compensator alloy installed as sheets between permanent magnet material bricks.

between the bricks. Since $\vec{H}_{||}$ is continuous across a boundary, we expect the same $\vec{H}$ but we expect to provide a flux of $\vec{B}$ with the ferrite and subtract flux with the compensator. The geometry has been employed to compensate the gradient magnet designed for the 8 GeV transfer line.

Following Halbach[7], we calculate the compensation effects with the same formalism as above.

$$B_g g = -\frac{\sum A_i B_{ri}}{\sum \frac{A_i \mu_{ri}}{h_i} + \sum E_j L_j \mu_0 V_m} \tag{31}$$

We justify this based on the linearity of the measured B-H curves for the compensator shown in Figure 7. We operate with H of about 1500 Oe ($\mu_0 H = 0.15$ T). However, the sign of H places the ferrite in the second quadrant of its B-H curve. It places the compensator in the third quadrant of its B-H curve. Since we will use data measured in the first quadrant, we will replace $B_r \rightarrow -B_r$ for the compensator data. We will also add a subscript at this point to distinguish the compensator (c) and ferrite (pm) properties.

$$B_g g = -\frac{\sum A_{pmi} B_{rpm} - \sum A_{ci} B_{rc}}{\sum \frac{A_i \mu_{ri}}{h_i} + \sum E_j L_j \mu_0 V_m} \tag{32}$$

Temperature effects of the geometry are small ($\sim 10^{-5}/^o$ C). We assume (and have measured) that $d\mu_r/dT$ is small. We will set the temperature derivative $d(B_g g)/dT = 0$. With the assumptions above, the denominator is temperature independent, yielding

$$\sum A_{pmi} \frac{dB_{rpm}}{dT} - \sum A_{ci} \frac{dB_{rc}}{dT} = 0 \tag{33}$$

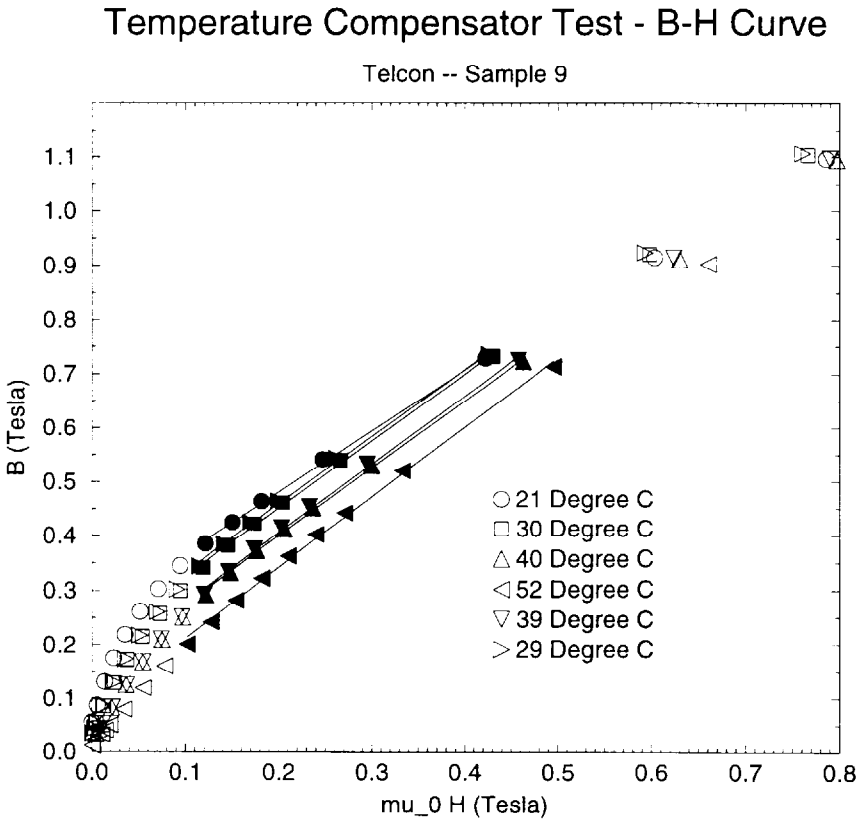

Figure 7: Measured B-H Curves for NiFe Compensator at various temperatures

Note that

- it is $\frac{dB_r}{dT}$ not $\frac{1}{B_r}\frac{dB_r}{dT}$ which establishes the compensator area.
- compensation is set by area ratios, not volume ratios, though the reluctance effects of the compensator gaps require consideration of the thickness to achieve a specified field strength.
- Calculations of requirements for ferrite (or other CSEM) or compensator will probably be carried out using Equation 32. However, when one has determined the proper ratios for the materials to be used, one can return to Equation 7, applying the property of the mixed material when continuing the design problem.

Using Equations 32 and 33 we can design a compensation system for temperature stabilization of the field strength. If the magnet has only indirect fields (all flux through the working portion of the gap emerges from iron), then the normalized field shape is temperature independent (even without compensation). From the NiFe temperature compensation alloy which is commercially available, we have selected one which provides $1/M\ dM/dT \sim -2\%/^oC$ and $B_{rc} \sim 0.25T$. We expect to provide a temperature compensation to $\sim 10^{-4}/^oC$ using these techniques. For many designs, We will mix ferrite bricks and compensator in a regular array along back side of the poletip. The $\vec{H}$ will be uniform, but the $\vec{B}$ will reverse at each boundary between ferrite and compensator. We have no precise measurements of compensator properties. Instead, we use a successive refinement approach to achieve precise field strength and temperature compensation based on measurement and tuning.

6 Trimming Magnet Strength

The integrated strength of storage ring magnets will need to be established with a relative accuracy of $10^{-3} - 10^{-4}$ depending on other details of the accelerator system design. For a fixed magnet geometry, we have shown that the strength is set by $\sum A_i B_{ri}$. The 0.15 T magnets which we are building are about 4 m long and use about 50 ferrite bricks (4″ by 6″) per pole. At fixed B_r, one creates strength changes of 2% by adding one brick.

Control at the 10^{-3} level can be achieved by fractional brick areas (A_i) or by careful control of B_r on some or all bricks (precision demagnetization). To achieve finer control of the pole strength to match the poles and to set the precise magnet strength will require further adjustment. Positive

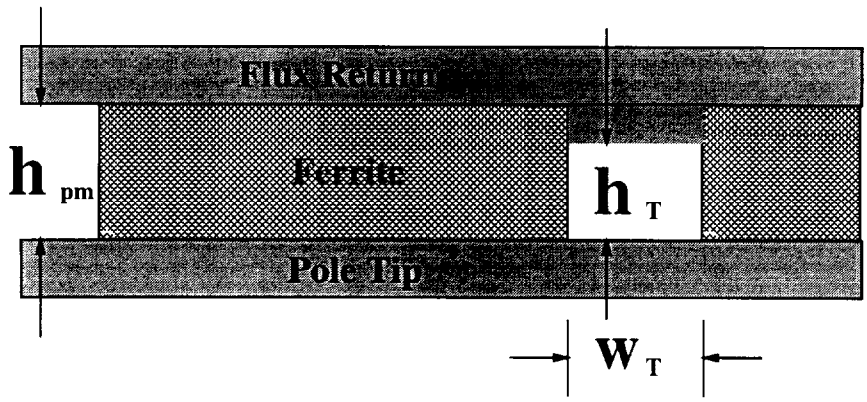

Figure 8: Arrangement of materials for an adjustable field strength trim using a flux shunting variable gap. For small shim one ignores the fact that non-perpendicular fields are introduced.

adjustment using movable (rotatable) ferrite pieces is an alternative which has not been pursued. Adjusting the permeance with a variable gap flux shunt is a straightforward solution, however.

Figure 8 illustrates a useful tuning geometry. We calculate with the same formula (Equation32), identifying separately the space (A_T) set aside for variable gap ($h = h_T - \delta$) trimming.

$$\mu_0 V_m = B_g g = -\frac{\sum A_i B_{ri}}{\sum \frac{A_i \mu_{ri}}{h_i} + \frac{A_T}{h_T - \delta} + \sum E_j L_j}. \tag{34}$$

Note that this is an approximation which assumes that all fields are transverse. We apply it to determine the magnitude of the area required for tuning. A more accurate analytical calculation is possible in the 2-dimensional approximation, but we will not pursue it here.

Identifying V_0 as the value of V_m when $\delta = 0$ we have

$$\frac{V_m}{V_0} = \frac{1}{(1 + \frac{\frac{A_T}{h_T - \delta} - \frac{A_T}{h_T}}{\sum \frac{A_i \mu_{ri}}{h_i} + \frac{A_T}{h_T} + \sum E_j L_j})} \tag{35}$$

$$\frac{V_m}{V_0} = \frac{1}{1 + \frac{1}{p_0}(\frac{A_T}{h_T - \delta} - \frac{A_T}{h_T})} = \frac{1}{1 + \frac{A_T}{p_0}(\frac{\delta}{h_T(h_T - \delta)})} \tag{36}$$

where p_0 is the permeance with the initial tuning position. Let $p_T = A_T/h_T$ be the initial permeance of the trim location and let us expand, keeping terms up to first order in δ, giving

$$\frac{V_m}{V_0} = 1 - \frac{p_T}{p_0}\frac{\delta}{h_T}. \tag{37}$$

Multiplying the potential by the permeance gives the flux through that permeance. Since the tuning area sees the pole potential, we can understand the tuning range by relating it to the total flux entering the pole.

$$\frac{V_m}{V_0} \approx 1 - \frac{\phi_T}{\phi_{total}}\frac{\delta}{h_T}. \tag{38}$$

One achieves a tuning range of 10^{-3} while varying the tuning gap by 25% if the fraction of flux shunted via the tuning gap is 4×10^{-3}. Flux compensation and strength tuning can use the same gap region.

7 Effects of Gaps in CSEM

The above calculations are easily extended to the case in which the space available for CSEM is not filled. Of greatest interest is the case in which a pole area A_i faces a gap whose total height is h_i but for which the portion adjacent to the pole has material 1 with height h_1 and the balance of the gap is filled with material 2 of height h_2. ($A_2 = A_1$). We again apply Ampere's Law but now we find

$$\frac{B_g g_h}{\mu_0} - h_1 H_1 - h_2 H_2 = 0. \tag{39}$$

By flux conservation, we know $B_1 = B_2 = B$. Using $B = B_r + \mu_r \mu_0 H$ for each material, and substituting in the above equation for H_1 and H_2 we have

$$\frac{B_g g_h}{\mu_0} - \frac{h_1}{\mu_0 \mu_{r1}}(B - B_{r1}) - \frac{h_2}{\mu_0 \mu_{r2}}(B - B_{r2}) = 0. \tag{40}$$

Before solving for B, let us simplify manipulations by expressing the heights as effective heights.

$$\frac{B_g g_h}{\mu_0} - \frac{h_1'}{\mu_0}(B - B_{r1}) - \frac{h_2'}{\mu_0}(B - B_{r2}) = 0. \tag{41}$$

Solving for B we find

$$B = \frac{B_g g_h + h_1' B_{r1} + h_2' B_{r2}}{h_1' + h_2'} \tag{42}$$

Substituting this result into the flux conservation equation gives

$$\sum \phi_i = \sum A_i B_i + A_1 \frac{B_g g_h + h_1' B_{r1} + h_2' B_{r2}}{h_1' + h_2'} + \sum \phi_{ei} = 0. \tag{43}$$

We will neglect the excess flux terms in the following steps.

$$\sum A_i (B_{ri} + \frac{B_g g_h}{h_i'}) + A_1 \frac{B_g g_h + h_1' B_{r1} + h_2' B_{r2}}{h_1' + h_2'} = 0. \tag{44}$$

$$\sum A_i B_{ri} + A_1 \frac{h_1' B_{r1} + h_2' B_{r2}}{h_1' + h_2'} + \sum A_i \frac{B_g g_h}{h_i'} + A_1 \frac{B_g g_h}{h_1' + h_2'} = 0. \tag{45}$$

At this point we will use the symbols P_i for the permeance and $R_i = P_i^{-1}$ for the reluctance of the region filled with material i. We solve for $B_g g_h$,

$$B_g g_h = \frac{\sum A_i B_{ri} + A_1 B_{r1} \frac{h_1'}{h_1' + h_2'} + A_2 B_{r2} \frac{h_2'}{h_1' + h_2'}}{\sum \frac{A_i}{h_i'} + \frac{A_1}{h_1' + h_2'}}. \tag{46}$$

$$B_g g_h = \frac{\sum A_i B_{ri} + A_1 B_{r1} \frac{R_1}{R_1 + R_2} + A_2 B_{r2} \frac{R_2}{R_1 + R_2}}{\sum R_i^{-1} + \frac{1}{R_1 + R_2}}. \tag{47}$$

We observe that the modified material changes the result in two ways. The permeance is changed, but this change is expected to be small. The driving flux is modified much like the change observed with a voltage divider circuit. If one of the materials is air, then we would obtain the correct result by adding a charge to the pole of the amount provided by the CSEM but also adding a sheet of charge with opposite sign on the other face of the CSEM. It subtracts from the net flux in proportion to the potential on the surface where it is placed.

These equations can be applied simply to some situations which are useful. When the CSEM is supplied in thicknesses which are half of the desired gap to the pole, one can use two pieces stacked in depth and average their properties. If less material is needed, a single piece provides half of the flux. For compensation, rather than filling an available gap with compensator material, one can reduce the total gap with iron shims, which will increase

the field, but leave an air gap between the iron and the compensator, to increase reluctance and thereby reduce the field and the compensation. This compensator design alternative permits one to optimize the cost of CSEM and compensator. For present efforts, neither ferrite nor compensator is a dominating cost so simpler designs have been selected.

8 Example Calculation: PDD Dipole

To illustrate these calculations, we will examine the design and performance of a dipole magnet series which will serve in the 8 GeV Transfer line from the Fermilab Booster to the Fermilab Main Injector (under construction). This magnet is designated PDD. It is required to provide a higher field strength to match the bend requirements of the tunnel. It achieves this with a "double-double" brick arrangement – two layers of bricks above the pole and two layers of bricks beside the pole. Figure 9 illustrates an end view of the design. In addition to the indirect fields which dominate the strength of this magnet, ferrite is employed to create direct fields in the gap. This ferrite is below the pole at the edge of the gap. It is used to shape the field in the gap. These "side" bricks add less flux to the pole than those in the positions above and below the pole which add in the fashion which was calculated above. The field uniformity requirements are not stringent so the space for compensator was selected where it bridges the gap, which much increases its effectiveness while leaving more space for ferrite bricks than is possible with the design illustrated in Figure 6. It is built with a 97 inch long pole tip iron and 101 inch long flux return iron. We will engage in a several step process to compare the calculations above to the observed performance of a series of these magnets.

8.1 Permeance Calculation

We begin with a calculation of the permeance. This is shown in Table 1. Details are presented for the purpose of letting the symmetry of the calculation assist in making the structure of the calculation apparent. The "ideal" flux is calculated with one term for each of six faces of the pole. The "excess" flux calculation produces two terms for each of the 12 edges of the pole. Only a few details are not treated fully. The ends are calculated as if there were a solid end plate. A plate with a hole for the beam is used. A permeability correction to excess flux on the sides is ignored. The ferrite bricks extend over much of the area considered for the excess flux calculation. This will

Calculate Upper Half Magnet						
Ideal Flux Terms						
Portion	Length	Width	Area	Gap	μ_r	Permeance
	inches	inches	m^2	inches		m
Pole Bottom	97	6.08	0.38049	1.015	1	14.7585
Pole top	97	6.08	0.38049	2.02	1.044	7.74209
Pole Left	97	0.965	0.06039	2.03	1.044	1.22275
Pole Right	97	0.965	0.06039	2.03	1.044	1.22275
Pole Label End	6.08	0.965	0.00379	2	1	0.07451
Pole Other End	6.08	0.965	0.00379	2	1	0.07451

Excess Flux Term						
Portion	h_1	h_2	a	E	L	Permeance
	inches	inches			inches	m
Pole Bottom rt	1.015	2.03	0.5	0.42345	97	1.04328
Pole Bottom lt	1.015	2.03	0.5	0.42345	97	1.04328
Pole top rt	2.02	2.03	0.99507	0.28004	97	0.68997
Pole top lt	2.02	2.03	0.99507	0.28004	97	0.68997
Pole top rt	2.03	2.02	1.00495	0.27869	97	0.68664
Pole top lt	2.03	2.02	1.00495	0.27869	97	0.68664
Pole Bottom rt	2.03	1.015	2	0.22009	97	0.54226
Pole Bottom lt	2.03	1.015	2	0.22009	97	0.54226
Label End rt	2.03	2	1.015	0.27735	0.965	0.0068
Label End lt	2.03	2	1.015	0.27735	0.965	0.0068
Label End rt	2	2.03	0.98522	0.28142	0.965	0.0069
Label End lt	2	2.03	0.98522	0.28142	0.965	0.0069
Other End rt	2.03	2	1.015	0.27735	0.965	0.0068
Other End lt	2.03	2	1.015	0.27735	0.965	0.0068
Other End rt	2	2.03	0.98522	0.28142	0.965	0.0069
Other End lt	2	2.03	0.98522	0.28142	0.965	0.0069
Label End tp	2.02	2	1.01	0.27801	6	0.04237
Other End tp	2.02	2	1.01	0.27801	6	0.04237
Label End bt	1.015	2	0.5075	0.41924	6	0.06389
Other End bt	1.015	2	0.5075	0.41924	6	0.06389
Label End tp	2	2.02	0.9901	0.28073	6	0.04278
Other End tp	2	2.02	0.9901	0.28073	6	0.04278
Label End bt	2	1.015	1.97044	0.22079	6	0.03365
Other End bt	2	1.015	1.97044	0.22079	6	0.03365
bottom	top	sides	end	ideal	excess	total
16.8451	9.1220	4.9033	0.5692	25.0951	6.344	31.4396

Table 1: Calculation of permeance of the magnetic structure of Fermilab PDD dipoles for the Booster to Main Injector 8 GeV transfer line. The calculation applies to the upper half of the magnet. Multiply by two to get the total permeance.

increase the permeance of those regions by 4.4%. If this applied to the full excess flux it would increase the permeance by less than 1%. The permeance

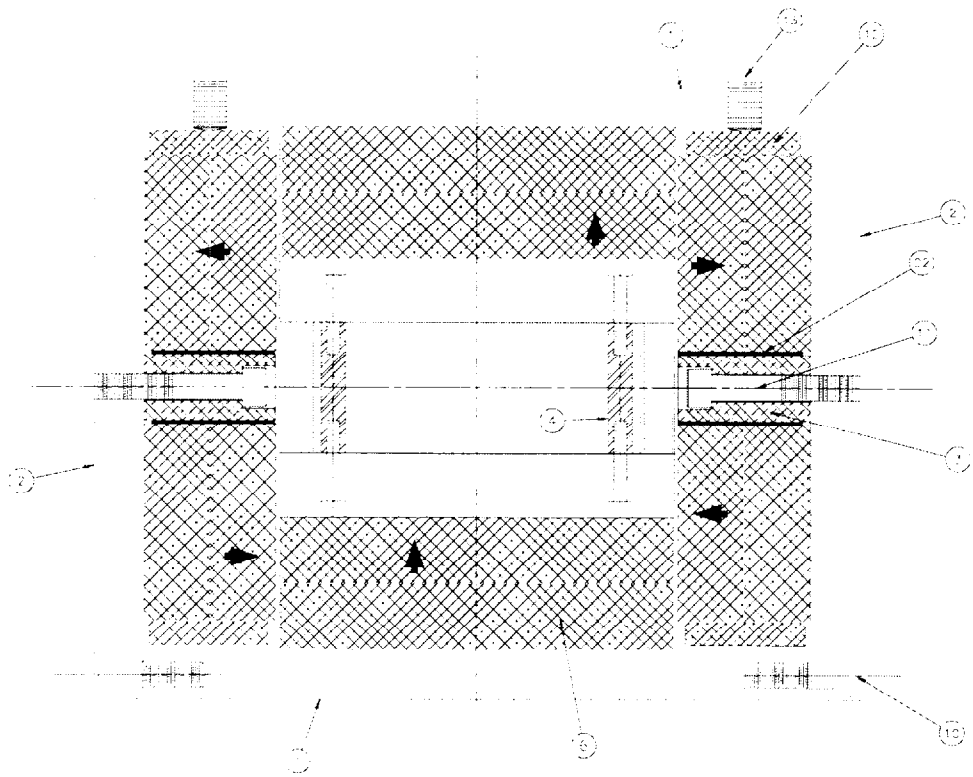

Figure 9: Schematic end view of the PDD magnet design. Items 1 & 2 are the flux return iron, Item 4 is the pole tip assembly, consisting of two pole tips, spacers, and compensator strips of 2″ high by 0.050″ wide NiFe temperature compensation material, Item 6 is a 6″ wide by 1″ high by 4″ deep ferrite (top or bottom) brick. Item 7 is a 3″ high by 1″ wide by 4″ deep ferrite side brick. Arrows indicate the direction of ferrite magnetization. Items 3, 12, & 22 are spacers.

Calibration Constants		
Brick Tester Calibration	9.23E-06	$T - m^2/gauss$
Probe LD1404 Effective Width	0.06604	m
Probe LD1404 Resistance	112.98	Ohms
Int Time constant (MTFIN210)	0.100532	sec
Int Capacitor (MTFIN210)	1E-06	farad
Measurement Time Constant	0.100645	sec
PDD Design Properties		
Compensator Width	0.050	inches
Compensator Length	97	inches
Compensator Strip Count	26	
PDD Pole (& Effective) Length	97	inches
PDD Half Gap	1.015	inches
PDD Permeance	62.8792	m

Table 2: Calibration constant and geometry for Calculation of Strengths for PDD019. Effective width of Flipcoil LD1404 is based on nominal 0.25″ aluminum form and 10 turns of 0.010″ wire.

of the region which contains compensator material has been accounted for above. The compensator permeability correction is larger ($\mu_r \approx 1.2$); the net effect would be to increase the PDD permeance by about 1%.

We have measured the flux provided by each brick in the assembly of these magnets. The compensator is not measured. We evaluate the strength of these magnets with a simple flipcoil system in the assembly facility at Fermilab Building MP9 and compare the results[7] with predictions above. After completing the assembly, the magnets are shipped to the Magnet Test Facility at IB#1 where the strength is confirmed with a well calibrated system. We will examine various contributions to the strength of PDD dipoles. Tables 2 and 3 provide the details.

[7]The measured integrator voltage (after drift correction) is assumed to be due to a flux change such that $\phi = VRC$ where RC is the time constant of the measurement system. The integrator calibration is made with low coil resistance. One adds to the calibration RC the product $C_{int}R_{coil}$. The value of $\int Bdl$ is given by $\int Bdl = \phi/2Nw$, where the 2 is due to flipping from positive to negative flux (180^o).

Results with no side bricks or compensator		
Brick Strength (top + bottom)	59674.8	"gauss"
Brick Strength (top + bottom)	0.55065	T-m^2
Flip Coil integrator Voltage	0.5529796	Volts
$\int Bdl$	0.4213705	T-m
B (in body)	.1710247	T
Pole Potential ($\mu_0 V_m$)	0.0044092	T-m
Measured Permeance	62.4436	m
Results with top/bottom bricks & compensator		
Measured Str w/26 Pieces	.453309	Volts
delta Strength w/ 26 Pcs	.0996706	Volts
delta Strength w/ 26 Pcs.	.075949	T-m
delta Pole Potential w/ 26 Pcs.	.0007947	T-m
Compensator Flux	.0496255	T-m^2
Compensator B_{rc}	.3049946	T
Results with completed dipole		
Measured Strength of Complete Dipole	.7916287	Volts
Contribution from Side Bricks	.3383197	Volts
$\int Bdl$ from Side Bricks	.2577997	T-m
Pole Potential from Side Bricks	.0026976	T-m
Side Brick Flux (Meas Permeance)	.1684476	T-m^2
Measured Sum from Side Bricks	55510	Gauss
Flux Available from Side Bricks	0.25611	T-m^2
Effective Flux Fraction (side)	0.6577	

Table 3: Calculation of Strengths for PDD019. Potentials are $\mu_0 V_m$.

8.2 Strength Contributions of Top and Bottom Bricks

As an initial step in evaluating these calculations, we assembled magnet PDD019 with only its top and bottom bricks installed. We evaluate the strength from a measurement of the $\int Bdl$ with a flip coil. For a permanent magnet, the effective length, L_{mag} is the same as the pole tip length (97″). The ferrite bricks were evaluated using the MTF Brick Tester[8] which was calibrated using the results from bricks which were measured by the supplier. The flux created by the top and bottom bricks is fully captured by the magnet pole so the contribution which they make is directly calculable from Equation 32. Each brick is measured individually. They are stacked two bricks high in the PDD design so the calculation averages the results for two bricks (the summed flux is divided by two).

We choose to compare measurement and calculation by measuring a permeance for the PDD design as a ratio of the flux from the bricks to the pole potential which they create (as measured by the integrated field). We find that the measured permeance is 0.7% lower than that calculated in Table 1. As noted above, the calculation fails to include small effects which would further increase the discrepancy by a further one or more percent. Random uncertainties in the measurement of $\int Bdl$ and of the bricks are thought to be of order 0.1 - 0.2%. Possible systematic and calibration errors in the brick tester are under evaluation at this time. For the balance of this calculation, we will use the permeance measured with the top and bottom bricks.

8.3 Strength Contributions of the Compensator

Figure 7 is based on additional measurements in the system described by Chen *et. al.*[9]. It may be subject to significant uncertainties so we choose to use measurements of PDD019 to evaluate the strength contribution of the compensator. The steps are shown in Table 3. Using the measured potential change as shown by the flipcoil measurement, and the permeance inferred above, we calculate the flux produced by the compensator. Using the compensator area, we infer a value for B_r. Note that the compensator bridges from the upper pole to the lower pole in this design, not from pole to the flux return. In effect each 2″ wide piece of compensator provides two 1″ compensators. For this reason we double the area of compensator in the calculation. The inferred value for B_r is larger than the room temperature value found in the fits to Figure 7, but within the systematic uncertainties

of that measurement.[8]

8.4 Strength Contributions of Side Bricks

The flux from the side bricks is not efficiently captured by the pole tip. Less than 1/3 of the brick face is in contact with the pole tip. Rather than utilizing the POISSON calculations of the PDD strengths, we will infer the contributions of the side bricks from the PDD019 measurements. From the measured change in pole potential, we infer the flux change due to side bricks from the previously measured permeance. We compare this to the measured flux produced by the bricks in the brick tester. Again, we average the two bricks which are stacked at each location by dividing the side brick sum by two. The overall side brick efficiency (65.77%) indicates that about half of the flux which is not directly captured by the side of the pole is effective in creating bending strength in this design.

9 Results from PDD Production

More than 40 PDD dipoles will be built. Using PDD008 - PDD016, we will examine the data on brick and magnet strength to further confirm the usefulness of the above calculations. As in the studies of PDD019, we will use the average flux produced by two bricks stacked on top of each other, with top and bottom bricks contributing at full strength and side bricks at 65.77%. The data will be presented in two ways. First, we will assume that all compensator contributes with an average B_r. We will compare the magnet strength predicted by the brick and compensator strength to the measured magnet strength. These results are shown in Figure 10. For magnets PDD008-015, the RMS deviation between measured and predicted strength divided by the mean measured strength is 0.23%. Equivalently, we will assume the bricks correlate perfectly with the measured strength and use the magnet strength as a measure of the B_{rc} of the compensator. A

[8] This measurement was performed at about 0.15 T fields. The compensator in the fully assembled PDD sits at about .245 T fields. Since the B-H line of the compensator is still curved in this region, the effective intercept (B_r) may be somewhat higher at higher fields. We expect that precise compensation should rely on detailed adjustment rather than precise measurements of the compensator properties. Nevertheless, we expect to monitor the strength and compensation properties in terms of the parameters which are identified in this calculation, expecting that they are both approximately correct, and that, within the range of designs under consideration, the model upon which this calculation is based is quite suitable.

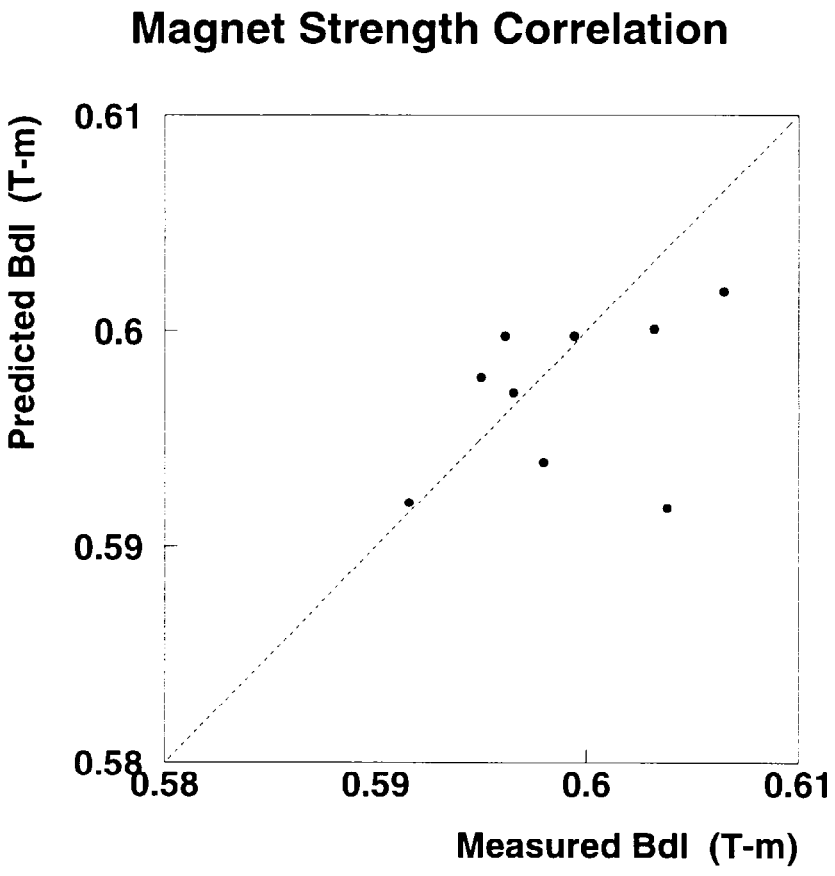

Figure 10: Comparison of the measured strength of PDD dipoles with a prediction assuming B_{rc} = .361 T. Magnet PDD016 shows the apparent poor correlation. Dashed line corresponds to ideal prediction. For magnets PDD008-015, the normalized RMS deviation between measured and predicted strength is 0.23%.

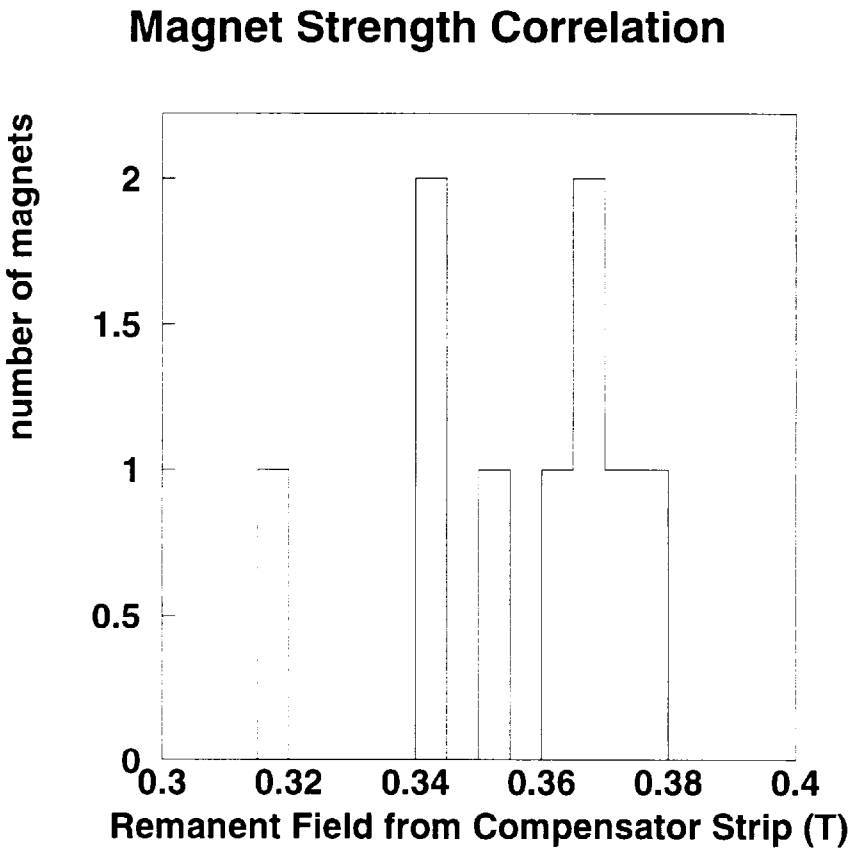

Figure 11: Apparent B_r of FeNi Compensator material as inferred from measurements of ferrite flux and magnet permeance in combination with the integrated bending field produced as measured by the flipcoil technique. Low value is the one inferred for PDD016.

histogram of the resulting B_{rc} is shown in Figure 11. The data for these magnets is provided in Table 4.

The production of PDD magnets is currently under study and additional results will be compiled separately. Of note is some information on compensation which is now know. We have measured many of these magnets at both room temperature and at $\sim 3^oC$. For most of them, the relative strength change is $\leq 2 \times 10^{-3}$, confirming that compensation has been carried out properly. More detailed studies indicate that we require 24 (26) compensator strips for PDD010 (PDD016), indicating that significant differences in compensator properties do exist. In Figure 11, the data for PDD010 lies in the group with larger values of B_r. As noted, PDD016 measurement would suggest that the compensator used for it has a lower B_r. If we assume perfect compensation and apply Equation 33, we find

$$\frac{dB_{rc}}{dT} = \frac{\sum A_{pmi} B_{rpm}}{\sum A_{ci}} \left(\frac{1}{B_{rpm}} \frac{dB_{rpm}}{dT} \right) \tag{48}$$

If we apply the weighted sum of the brick strengths and assume

$$\frac{1}{B_{rpm}} \frac{dB_{rpm}}{dT} = -.002, \tag{49}$$

Ser	Side	Top/Bot	Weighted	#	Predicted	Measured	Comp
#	Brick	Brick	Brick	Comp	Magnet	Magnet	B_{rc}
	Flux	Flux	Flux	Strips	Strength	Strength	
	gauss	gauss	T-m^2		T-m	T-m	T
8	54914	59599	.88326	12	0.5929	0.5878	0.3669
9	55237	60013	.88904	12	0.5973	0.5929	0.3636
10	55561	60162	.8924	12	0.5999	0.5923	0.3774
11	55029	59749	.88534	12	0.5945	0.5932	0.3500
12	55597.3	60253	.8934	12	0.6007	0.5951	0.3689
13	55297.4	60005.4	.88933	12	0.5976	0.5907	0.3744
14	55950.3	60834.8	.90095	13	0.5995	0.5999	0.3440
15	55862.9	60253.1	.89505	12	0.6019	0.6022	0.3428
16	55323.7	60133	.89067	13	0.5917	0.5987	0.3172

Table 4: Measured properties of selected PDD dipoles at the end of initial production. Strength trimming was applied subsequent to the strength measurement.

we find values of dB_{rc}/dT of 0.00547 T/°C (0.00594 T/°C) for PDD016 (PDD010). These are of the same magnitude but not as high as the values reported by the manufacturer for measurements at 50 Oe.

10 Effects of Steel Properties

Effects due the the finite permeability of steel are often not large in hybrid permanent magnets since one is dealing with intermediate fields where neither the remanent field nor large H values associated with saturation are important. Since the effects are small, we are satisfied to find an estimate for their size. In the same spirit as the balance of this calculation, we will consider the effects on a dipole of the steel pole and flux return in the approximation that for that for steel

$$B = \mu_0 \mu_l (H - H_c) \tag{50}$$

where μ_l is the relative permeability of steel. If we parameterize low carbon steel with this form, we may expect H_c less than 3 Oe ($\mu_0 H_c < 0.0003$ T) and, for $B < 1T$, $\mu_l > 2000$. This approximation is useful for typical magnet iron below about 1 T.

To illustrate this calculation while keeping the algebra less cluttered, we will consider again a magnet like Figure 1 but assume that h_1 and h_3 are sufficiently large that we can neglect the flux through those sides of the magnet. We will label the thickness of the flux return steel as t_1, t_2, and t_3. Following the same method, we use Ampere's Law on a path beginning in the center of the gap and extending through the CSEM above the pole, then to the right through the upper and right side return yoke to the mid-plane. The return portion which follows the mid-plane to the starting point adds no contribution.

$$\frac{B_g g_h}{\mu_0} + \int_0^{w_1} H_{pole}(y)dy - h_2 H_2 + \int_0^{w_2/2} H_{ret}(x)dx + \int_{w_1}^{0} H_{ret}(y)dy = 0. \tag{51}$$

We will substitute for H using Equation 50. In both vertical segments, B is uniform and given (using flux conservation) by

$$B_{pole}(y) = B_g \quad B_{ret}(y) = \frac{B_g w_g}{2t_1} \tag{52}$$

Along the top we assume that the field increases linearly since the return yoke has constant thickness and flux is added in linearly.

$$B_{ret}(x) = \frac{B_g x}{t_2} \tag{53}$$

with x,y measured from the center of the gap. Substituting for H and performing the integration we have

$$\frac{B_g g_h}{\mu_0}+H_c w_1+\frac{B_g}{\mu_0\mu_l}w_1-h_2\frac{B_2-B_r}{\mu_0\mu_r}+H_c\frac{w_2}{2}+\frac{B_g}{\mu_0\mu_l}\frac{w_2^2}{8t_2}+H_c w_1+\frac{B_g}{\mu_0\mu_l}\frac{w_1 w_g}{2t_1}=0. \quad (54)$$

$$\frac{B_g g_h}{\mu_0}+H_c(2w_1+\frac{w_2}{2})+\frac{B_g}{\mu_0\mu_l}(w_1+\frac{w_2^2}{8t_2}+\frac{w_1 w_g}{2t_1})-h_2\frac{B_2-B_r}{\mu_0\mu_r}=0. \quad (55)$$

Solving for B_2 we have

$$B_2=\mu_r\frac{B_g}{h_2}(g_h+\frac{1}{\mu_l}(w_1+\frac{w_2^2}{8t_2}+\frac{w_1 w_g}{2t_1}))+B_r+\mu_0\mu_r\frac{H_c}{h_2}(2w_1+\frac{w_2}{2}). \quad (56)$$

Substituting into the flux conservation equation we have

$$0=B_g w_g+\mu_r\frac{B_g w_2}{h_2}(g_h+\frac{1}{\mu_l}(w_1+\frac{w_2^2}{8t_2}+\frac{w_1 w_g}{2t_1}))+B_r w_2+\mu_0\mu_r\frac{H_c w_2}{h_2}(2w_1+\frac{w_2}{2}). \quad (57)$$

Solving for $B_g g_h$ we find

$$B_g g_h=-\frac{B_r w_2+\frac{\mu_0\mu_r H_c w_2}{h_2}(2w_1+\frac{w_2}{2})}{\frac{w_g}{g_h}+\mu_r\frac{w_2}{h_2}(1+\frac{1}{\mu_l g_h}(w_1+\frac{w_2^2}{8t_2}+\frac{w_1 w_g}{2t_1}))}. \quad (58)$$

We find that the iron modifies the results found in Equation 7 (or Equation 75) in two ways. The source flux is incremented by the flux which is driven across gap 2 by H_c. As usual, the field added across Gap 2 is proportional to the iron path length divided by a gap height. The permeance is modified by an additive term proportional to $1/\mu_l$. Since the coercivity depends upon the excitation history, the observed field contribution from the coercivity of the steel may depend strongly on details of assembly and/or previous magnetization history of the iron, if any. In no case would we expect a large contribution from the term which depends upon μ_l.

11 Higher Order Multipoles

We have seen that the strength calculation involves relating the desired field strength to the magnetic scalar potential. In turn, this potential is determined by the flux supplied by the CSEM and the permeance of the structure. To understand simple multipole structures, we will need formulas for the gap permeance and the relation between the pole potential and the

multipole field. We will consider a symmetric 2N-pole structure. We will examine a single pole of this structure beginning with the center of the multipole and extending in the angular region from 0 to π/N. An iron pole tip centered at $\pi/2N$ is placed at radius a. The poletip is shaped to form the equipotential for the multipole $2N$. We assume that the field created is precisely the desired multipole. The poletip is terminated adjacent to the x axis at $x = \alpha a$ and symmetrically along the other edge. Notice that the gap at the bottom of the dipole structure which we have examined has this form with $N = 1$.

The simple form of the multipole field permits us simple calculations. We relate the design strength of the multipole field, B_N, to the pole potential by observing that at angle $\pi/2N$ (where the pole is centered), the field is entirely radial. The line integral is then

$$\mu_0 V_m = \int \vec{B} \cdot d\vec{\ell} = \int_0^a B_N r^{N-1} dr = \frac{1}{N} B_N a^N. \tag{59}$$

To calculate the flux which enters the pole, we will choose to calculate twice the flux which crosses the x axis, since the same flux will also cross at π/N. The simplicity comes from the fact that all fields are tangential along the x axis.

$$\phi = 2\int_0^{\alpha a} B_\theta dr = 2\int_0^{\alpha a} B_N r^{N-1} dr = \frac{2}{N} B_N (\alpha a)^N \tag{60}$$

The (2-dimensional) permeance contribution from this multipole gap is given by the ratio of flux to potential.

$$P = \frac{\phi}{\mu_0 V_m} = 2\alpha^N. \tag{61}$$

To complete the calculation for this pole, one needs to describe the remaining iron, gaps, and CSEM. The contribution to the permeance from the pole region is simply added to other parallel permeances.

Calculations for gradient magnets can be well approximated by the calculation for a similarly shaped dipole.

12 Summary and Conclusions

We have shown that the magnetic scalar potential on the pole of a compensated hybrid permanent magnet is given by

$$\mu_0 V_m = -\frac{\sum A_{pmi} B_{rpm} - \sum A_{ci} B_{rc}}{\sum p_i + \sum L_j E_j} \tag{62}$$

where A_i is the area of a portion of the pole tip, p_i the corresponding permeance due to "ideal" flux, $L_j E_j$ the permeance due to "excess" flux term where E_j is the excess flux coefficient for edge j and L_j is the length of that edge. $A_i B_r$ is the flux added (subtracted) by the permanent magnet (compensator) material.

The corresponding design field is given by

$$B_N = \frac{N \mu_0 V_m}{a^N} \tag{63}$$

where 2N is the number of poles for the design field. N=1 for dipole. a is the pole radius for multipoles or the half gap for dipoles. This magnet will be thermally compensated provided

$$\sum A_{pmi} \frac{dB_{rpm}}{dT} = \sum A_{ci} \frac{dB_{rc}}{dT} \tag{64}$$

In summary we have shown that

- Analytic calculations provide detailed design formulas which relate geometry and magnetic material properties to the magnet strength. For hybrid permanent magnet designs which are suitable for accelerator use, we have demonstrated understanding at the 1% level.
- Flux Shunting for Temperature Compensation as suggested by Bertsche *et. al.*[10] can stabilize the strength changes with temperature, We have derived formulas which permit detailed design and understanding of temperature compensation systems.
- Setting the magnet strength by adjusting the total flux available from the permanent magnet material (CSEM) is a useful production technique.
- Further trimming of the strength is available using flux shunting techniques.

Experimental success of these techniques has been demonstrated.

13 Acknowledgments

This work documents a technique for understanding hybrid permanent magnets which is taught by Klaus Halbach. I would like to especially thank Dr.

Halbach for his help in understanding this material. G. William Foster and Gerald P. Jackson have guided the Fermilab effort in permanent magnets and have specified the designs under study. James Volk and Henry Glass have guided magnet fabrication and testing. Special thanks to Ira Friedman and Tom Egan, associated with the Fermilab TRAC summer program for teachers, for help with measurements and data management.

A Calculations for Simple Dipoles

A.1 Simple Plate Magnet

We will illustrate the technique for calculating the strength of a hybrid permanent dipole with a very simple geometry. We will then build on that to obtain useful formulas which account for more effects, allowing precise calculations. Figure 12 provides a very simple geometry. Assume that we are driving the field in a gap of height g and width w_g using a brick of CESM (ferrite) materials of height h $(= g)$ and width w_{pm}. In order to obtain

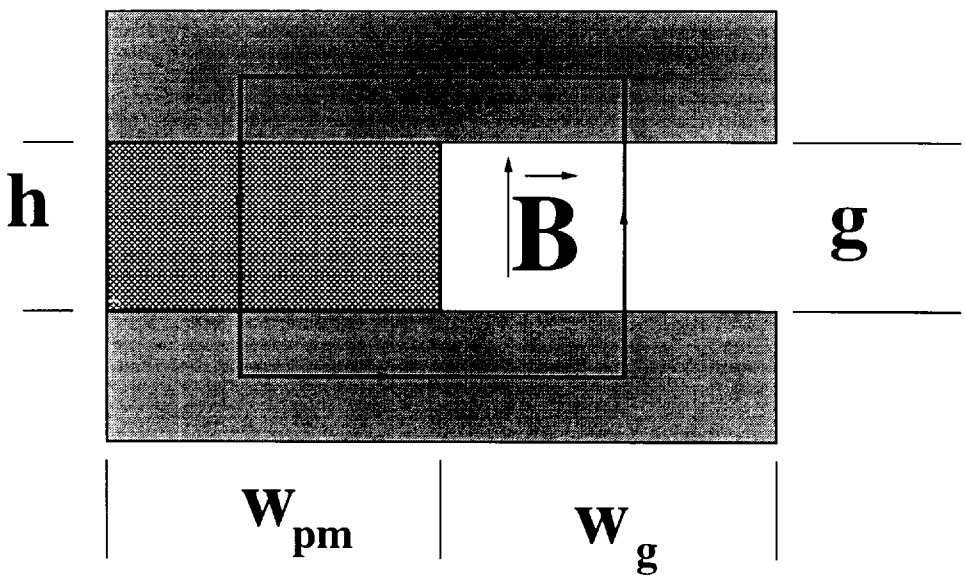

Figure 12: Schematic end view of a simple permanent magnet. Top and bottom plates are iron. Field is driven by brick of CSEM (ferrite) material placed between the plates.

simple, illustrative formulas, we will solve the one-dimensional problem in which we neglect the horizontal components of B in the gaps and assume that the boundaries are sharply defined at the edges. We will use two of Maxwell's Equations. We apply the conservation of magnetic flux on the external surface of the upper pole (iron).

$$B_g w_g + B_{pm} w_{pm} = 0 \tag{65}$$

since (by assumption) the field is zero except on the two inner surfaces. We apply Ampere's Law on the path shown. No current is enclosed by the path. We note that due to the high permeability of the iron, the H is small for the given $B.$, and the contribution from the portions of the path in iron is negligible, giving

$$\frac{B_g g}{\mu_0} - h H_{pm} = 0 \tag{66}$$

The problem has 4 unknowns - B and H in the gap and in the CSEM (ferrite). The two additional equations are provided by the magnetic property (constitutive) equations for the materials. In the gap we have $B = \mu_0 H$. The properties of a typical CESM material is shown in Figure 2 which a a B-H curve for strontium ferrite. We will be operating in the region $\mu_0 H > -.27$ T where the ferrite properties are well approximated by $B = B_r + \mu_r \mu_0 H = 0.400 + 1.044 \mu_0 H$. We define μ_r as the recoil differential permeability of the CSEM material[9]. The values of B_r and μ_r are typical of oriented strontium ferrite when magnetized to saturation.

We will characterize the iron surfaces by their magnetic potential, $\mu_0 V_m$ where $\frac{\mu_0 dV_m}{dy} = B_y$. B_y is uniform and, defining the potential reference (zero) on the lower pole, for the upper pole we find $\mu_0 V_m = B_g g$. We will solve for this using the expressions above. We solve for H_{pm} in the expression from Ampere's Law and substitute for H_{pm} in the equation for the CSEM properties. Substituting into the flux conservation equation, we have

$$B_g g \frac{w_g}{g} + (B_r + \mu_r \frac{B_g g}{h}) w_{pm} = 0 \tag{67}$$

$$B_g g \frac{w_g}{g} + B_g g \mu_r \frac{w_{pm}}{h} = -B_r w_{pm} \tag{68}$$

[9]The literature on permanent magnets (*e.g.* Parker and Studders[11]) defines a recoil permeability as the average slope of a minor hysteresis loop. For those materials for which the B-H (demagnetization) curve has no useful linear portion in the second quadrant, there is still a nearly linear response on minor hysteresis loops. The distinction between recoil (minor loop) and differential (major hysteresis loop) slope is not significant for CSEM materials.

$$\mu_0 V_m = B_g g = -\frac{B_r w_{pm}}{(\frac{w_g}{g} + \mu_r \frac{w_{pm}}{h})} \tag{69}$$

This equation establishes the potential and thereby the dipole strength of this magnet in terms of the source term, determined by the remanence (B_r) of the CSEM and its width (area in the 3-dimensional case) divided by a permeance (reluctance^{-1}) for the geometry of the structure. The magnetic permeance is governed by a width (area) divided by the gap. In general, the permeance of the region with CSEM is modified slightly by the differential permeability of the CSEM. This can be accounted for by using an effective gap height

$$h_{eff} = \frac{h}{\mu_r} \tag{70}$$

The designer must also be aware of the "demagnetizing" field seen by the CSEM. The coercivity of the CSEM ($\mu_0 H \approx 0.27T$ for the ferrite shown in Figure 2) limits the field which can be supported without demagnetizing the CSEM. The relation between B_{pm} and H_{pm} is determined by the geometry of the magnetic circuit. Beginning with the expression derived from Ampere's Law (Equation 66) and replacing B_g using flux conservation (Equation 65) we have

$$B_{pm} = -\frac{\frac{w_g}{g}}{\frac{w_{pm}}{h}} \mu_0 H_{pm} \tag{71}$$

This "load line" can be imposed on the BH curve for the CSEM (such as Figure 2). The operating point will be the intersection of the two lines.

A.2 Simple Calculation for Rectangular Dipole

A useful geometry for a dipole which bends a particle beam is illustrated in Figure 13. We will ignore corners and ends to concentrate on the major effects. The fundamental equations are Maxwell's Magneto-static Equations: Ampere's Law and the Flux Conservation Equation. We apply the flux conservation with the notation that the magnetic field points toward the poletip in each gap. If we ignore edge effects, the results for each side of the pole are elementary.

$$B_g w_g + B_1 w_1 + B_2 w_2 + B_3 w_3 = 0 \tag{72}$$

By construction, the midplane (bottom of picture) is an equipotential surface at the same magnetic potential as the flux return shell. We apply Ampere's Law by following a flux line which begins on that surface, crosses

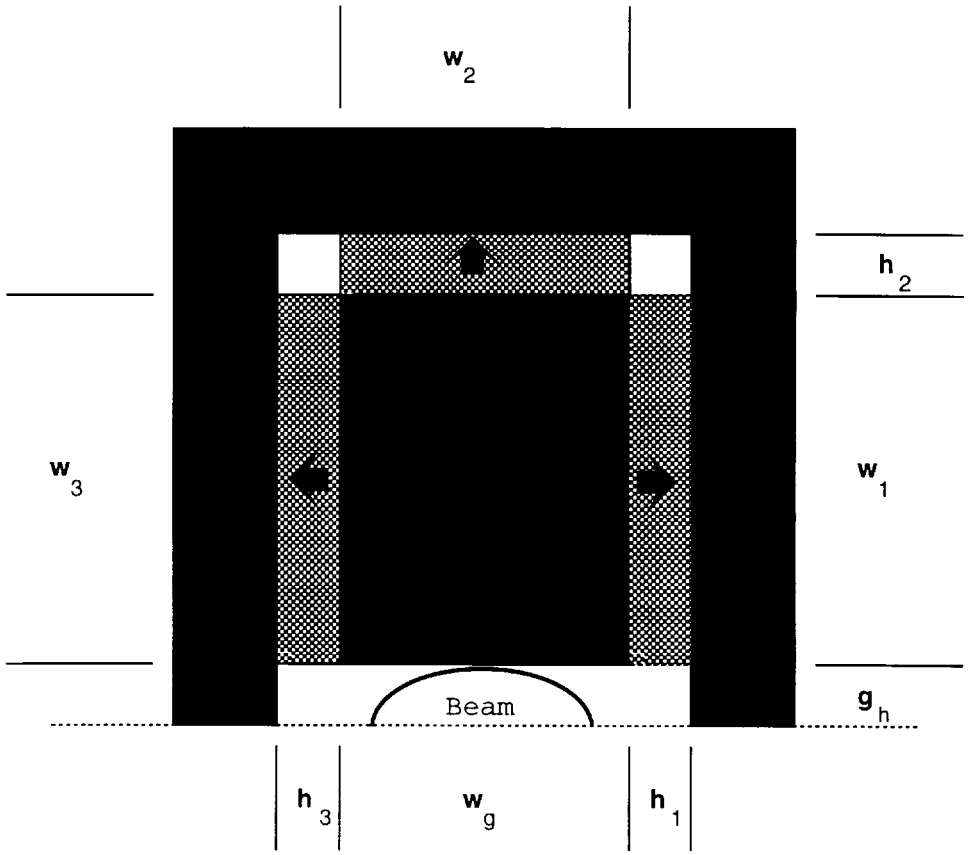

Figure 13: Schematic end view (upper half) of a permanent magnet hybrid dipole. The useful volume is in the gap above the centerline (shown at the bottom of the illustration. The pole tip is the iron block above the gap. Top, bottom, and side plates are iron for flux return. Field is driven by brick of CSEM (ferrite) material placed between the flux return plates and the pole tip.

the gap (half-gap height g_h) to the pole tip. Since the pole is assumed an equipotential, H is zero across that portion of the path. We then follow the flux line across the CSEM material in the top of the circuit to the flux return shell.

$$\frac{B_g g_h}{\mu_0} - h_2 H_2 = 0. \tag{73}$$

Following different flux lines, we will obtain the same form of equations for H_1 and H_3. We now wish to relate B and H. In vacuum (air) we have $B = \mu_0 H$ but for the CSEM permanent magnet material, we will be using strontium ferrite. A measured $B - H$ curve for this material is shown in Figure 2. We will be operating on the highly reversible linear portion of the curve where

$$B = B_r + \mu_0 \mu_r H. \tag{74}$$

Where B_r and μ_r are the intercept and slope of a line through that portion of the $B - H$ curve (plotted as B *vs.* $\mu_0 H$).

The solution is given by

$$B_g = -\frac{1}{g} \frac{(w_1 B_r + w_2 B_r + w_3 B_r)}{(\frac{w_g}{g} + \frac{\mu_r w_1}{h_1} + \frac{\mu_r w_2}{h_2} + \frac{\mu_h w_3}{h_3})} \tag{75}$$

We note that in describing this in three dimensions, we can simply multiply the numerator and denominator by the length L. We then replace $w_i L$ with A_i, the area of the region of interest.

When multiplied by the magnet length L, the denominator of the second fraction is known as the permeance of the magnet. Permeance is the inverse of magnetic reluctance. The numerator (multiplied by L) is the available flux. B_r is an effective density of magnetic charge. In this design the positive charges are deposited on the pole tip with the negative charges on the return yoke. Since the material is so linear, and the μ_r at high field is so near to 1, one can quite precisely design by choosing to place magnetic charge is appropriate places.

References

[1] K. J. Bertsche, B. C.Brown, and H. D. Glass. Flux Shunts for Temperature Compensation and Tuning in Ferrite Hybrid Permanent Magnets. *Bull. Am. Phys. Soc.*, 41:943, 1996. #G12-6.

[2] *Standard Specification for Permanent Magnet Materials.* Magnetic Materials Producers Association, 11 S. LaSalle St. Suite 1400, Chicago, IL 60603, 1985,1993. MMPA Standard No. 0100-90.

[3] G. W. Foster, K. Bertsche, J. F. Ostiguy, B. Brown, H. Glass, G. Jackson, M. May, D. Orris, and Dick Gustafson. Permanent Magnet Design for the Fermilab Main Injector Recycler Ring. In *Proceedings of the 1995 IEEE Particle Accelerator Conference, Dallas, May 1-5, 1995*, page 1298. Institute of Electrical and Electronic Engineers, 1995.

[4] G. Jackson. Recycler Ring Conceptual Design Study. TM 1936, Fermilab, July 1995.

[5] Malcolm McCaig. *Permanent Magnets in Theory and Practice.* Pentech Press, Estover Road, Plymouth, Devon, 1977.

[6] K. Halbach. Insertion Device Design: Sixteen Lectures Presented from October 1988 to March 1989. LBL 36183, Lawrence Berkeley Laboratory, March 1989.

[7] Klaus Halbach. Compensation of the Temperature Coefficient in a Hybrid Permanent Magnet. Technical Report MTF-95-0025 1.1, Fermilab, July 1995.

[8] Bruce Brown, G. William Foster, Darryl Orris, and James Volk. The MTF Permanent Magnet Brick Tester. Technical Report MTF-96-0004, Fermilab, October 1996.

[9] Wufei Chen, Carl Draeger, Darryl Orris, and Bruce C. Brown. B-H Curves of Some Magnet Material for Temperature Compensation. Technical Report MTF-95-0017 1.1, Fermilab, September 1995.

[10] K. Bertsche, J. F. Ostiguy, and G. W. Foster. Temperature Considerations in the Design of a Permanent Magnet Storage Ring. In *Proceedings of the 1995 IEEE Particle Accelerator Conference, Dallas, May 1-5, 1995*, page 1381. Institute of Electrical and Electronic Engineers, 1995.

[11] Rollin J. Parker and Robert J. Studders. *Permanent Magnets and Their Application.* John Wiley and Sons, Inc, New York, London, Sydney, 1962.